Transition Metal Hydrides as Electron Donors. Formation, Detection, and Dimerization of Transient, Paramagnetic Radical Cations from the Electrochemical Oxidation of Tungstenocene Hydrides and the Crystal Structure of the Binuclear $(Cp_2W)_2H_3^+$ Product

R. J. Klingler, J. C. Huffman, and J. K. Kochi*

Contribution from the Department of Chemistry and the Molecular Structure Center, Indiana University, Bloomington, Indiana 47405. *Received June 11, 1979*

Abstract: The electrochemistry of a variety of transition-metal hydrides, especially those derived from tungstenocene, shows that transient, paramagnetic radical cations are formed anodically at less than 0.4 V vs. SCE. The cyclic voltammogram of $Cp_2W(Ph)H$ is reversible at high sweep rates to produce the paramagnetic cation $Cp_2W(Ph)H^+$, which can be detected by ESR spectroscopy and is estimated to have a half-life of less than 30 s in solution. The radical cation from Cp_2WH_2 is too transient to be observed directly, but evidence for its formation was obtained by ac polarography at −77 °C and it can be readily trapped as the spin adduct to phenanthroquinone. Proton loss is a common fate of paramagnetic transition metal hydride cations, and the resultant neutral, metal-centered radical is subject to ready dimerization or reductive elimination. The binuclear $[CpMo(CO)_3]_2$ and $(Cp_2W)_2H_3^+ClO_4^-$ can be isolated from the anodic oxidation of $CpMo(CO)_3H$ and Cp_2WH_2, respectively. The X-ray crystal determination of $(Cp_2W)_2H_3^+$ shows an unusually long W–W distance of 3.628 Å and a symmetrical conformational distortion about each Cp–W–Cp unit which strongly suggest the presence of both bridging and terminal hydrides in the molecular structure, $Cp_2W(H)$–H–$(H)WCp_2$. The radical cation from $Cp_2W(Ph)H$ affords benzene in high yields, but deuterium-labeling studies with $Cp_2W(C_6D_5)D$ show that C_6D_6 is only a minor product compared to C_6D_5H. Deprotonation as an important step in the spontaneous decomposition of metal hydride cations is confirmed by pH methods and the isolation of acid salts.

Introduction

Transition-metal hydrides are the principal intermediates in a number of catalytic processes, including the hydrogenation of multiple bonds, hydroformylation of olefins, and the reduction of organohalogen compounds.[1] Only limited quantitative information is extant, however, as to how the metal hydrides react, particularly with regard to their interaction with the various substrates present in the catalytic reactions. In an earlier study, we showed that diamagnetic metal hydrides from the main-group elements (Si, Ge, and Sn) are excellent electron donors, and readily participate in charge-transfer interactions.[2] This investigation was undertaken to establish the feasibility of a similar electron transfer from transition-metal hydrides[3] and to employ electrochemical and electron spin resonance techniques to identify transient, paramagnetic intermediates. The isolation and characterization of the products derived from these metastable metal hydride radical cations are also important objectives of this study.

Results

I. Transition-Metal Hydrides as Electron Donors. Electrochemical oxidation is a useful technique to evaluate the electron-donor properties of the various types of metal hydrides included in Table I. In all cases, the first anodic wave occurred at an applied potential of less than +0.40 V relative to SCE. The ease of electron detachment from metal hydrides such as in eq 1 is indicated by the value of the anodic peak potential

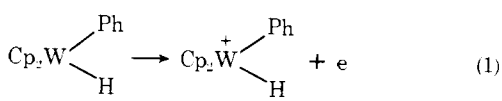

(1)

$E_p(a)$ in column 2. The reversible electrode potential E^0 was obtained by cyclic voltammetry at a stationary platinum electrode. For example, the cyclic voltammogram of tungstenocene phenyl hydride in Figure 1 shows both anodic and cathodic waves of equal magnitude [i.e., the peak current ratio, $i_p(a)/i_p(c) = 1.01$], which are separated by the theoretical value of 59 mV expected for a reversible electrochemical couple. However, the cyclic voltammetry of the analogous tungstenocene dihydride is only partially reversible even at −78 °C, showing only a small cathodic wave [$i_p(c)/i_p(a) = 0.15$] at sweep rates as fast as 10 V s^{-1}. The absence of a cathodic wave following anodic oxidation of some of the metal hydrides in Table I is related to the instability of the radical cation as we will elaborate in the next section.

II. Paramagnetic Cations of Transition-Metal Hydrides. Detection and Stability. The radical cations derived from the anodic oxidation of the diamagnetic metal hydrides in Table I are all too transient to be isolated as stable complexes. However, we wish to discuss how these paramagnetic species can be (1) identified in solution by electron spin resonance spectroscopy, and (2) their stability evaluated, particularly with regard to (3) decomposition by facile loss of a proton.

A. Direct Observation. The cation $Cp_2W(Ph)H^+$ is too transient to observe its electron spin resonance spectrum by conventional means. Instead, a flow electrochemical cell utilizing a microporous silver electrode[5] was inserted directly into the ESR cavity, and a solution of $Cp_2W(Ph)H$ in acetonitrile was continuously electrolyzed at +0.06 V vs. SCE and −45 °C. The ESR spectrum in Figure 2 (left) disappears immediately when the current is turned off, and its relatively high signal-to-noise level indicates a relatively stable but transient species. The doublet splitting of 12 G can be unambiguously assigned to the proton bonded to tungsten, since deuterium substitution affords the spectrum in Figure 2 (right).[6] [The singlet absorption of the deuterated analogue $Cp_2W(Ph)D^+$ results from the reduction of the doublet splitting by a factor of 6.51 ($=g_H/g_D$) to a value less than 2 G, which is unresolved within the envelope of the natural line width of more than 6 G.]

The cation derived from tungstenocene dihydride is too transient to observe directly even by these techniques. However, the paramagnetic species can be trapped as the phenanthroquinone PQ adduct (see Experimental Section) (eq 2). Thus the ESR spectrum shown in the top of Figure 3 corresponds to the addition of the paramagnetic monohydride

0002-7863/80/1502-0208$01.00/0

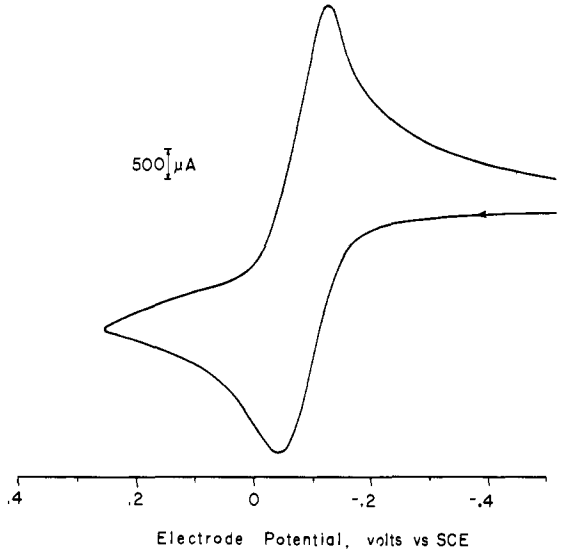

Figure 1. First scan cyclic voltammogram of 1.8×10^{-3} M $Cp_2W(Ph)H$ in acetonitrile containing 0.10 M tetraethylammonium perchlorate at a platinum microelectrode with a scan rate of 200 mV s^{-1}.

Table I. Cyclic Voltammetric Data for Selected Transition Metal Hydride Complexes[a]

metal hydride	$E_p(a)$	E^0	$i_p(c)/i_p(a)$[b]	Δ,[c] mV
$Ta(dmpe)_2(CO)_2H$[d]	−0.650	−0.688	1.00	75
$Fe(diphos)_2H_2$	−0.410		0	
Cp_2WH_2	−0.020	−0.350[e]	0	
$Cp_2W(Ph)H$	−0.060	−0.090	1.01	59
$Ir(PPh_3)_2(CO)H$	+0.130	+0.073	1.01	90
$Rh(PPh_3)_2(CO)H$	+0.135		0	
$Ru(PPh_3)_2(CH_3CO_2)H$	+0.230		0	
$CpMo(CO)_3H$	+0.360		0	

[a] Measured at 25 °C in acetonitrile with $[Et_4N][ClO_4]$ as supporting electrolyte. Voltage relative to saturated NaCl SCE. [b] Peak current ratio of the cathodic and anodic waves. [c] Voltage separation of cathodic and anodic peaks at a sweep rate of 100 mV s^{-1}. [d] See ref 4 for a list of abbrevations. [e] Measured at −77 °C in acetone-acetonitrile by ac polarography.

Cp_2WH (resulting from the deprotonation of $Cp_2WH_2^+$) to phenanthroquinone. The presence of only one hydrogen still

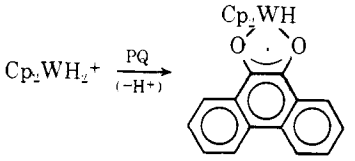

(2)

bonded to tungsten in the adduct is confirmed by the computer-simulated spectrum shown in the bottom of Figure 3. The ESR parameters of this PQ adduct are compared with those of the related PQ adducts[7] from $(OC)_4Mn$ and $(CH_3)_3Sn$ in Table II.

B. Lifetimes of Tungstenocene(III) Radicals. A Comparison. The group of structurally similar, paramagnetic d^1 organometallic species derived from tungstenocene in Table III exhibits a wide range of radical lifetimes. For example, $Cp_2WH_2^+$ is too unstable at 25 °C to be detected directly, and its lifetime, based on double step chronoamperometric studies, is less than 1 ms. Indeed, the plot of the anodic peak potential vs. the sweep rate (log v) in Figure 4 has a slope of 58 mV per decade, indicative of a process in which electron transfer is actually rate limiting.[8] At −78 °C, there is some evidence for reversibility at high sweep rates, but the peak current ratio of the cathodic to anodic wave $i_p(c)/i_p(a)$ does not exceed 0.15 even at 10 V s^{-1}. The fundamental-harmonic ac polarographic wave at −77 °C is reversible in the frequency range 250–1000 Hz (see Experimental Section for details). Using the lower limit, the lifetime of the cation radical may be estimated to be 4 ms at −77 °C.

The phenyl analogue $Cp_2W(Ph)H^+$ is sufficiently more

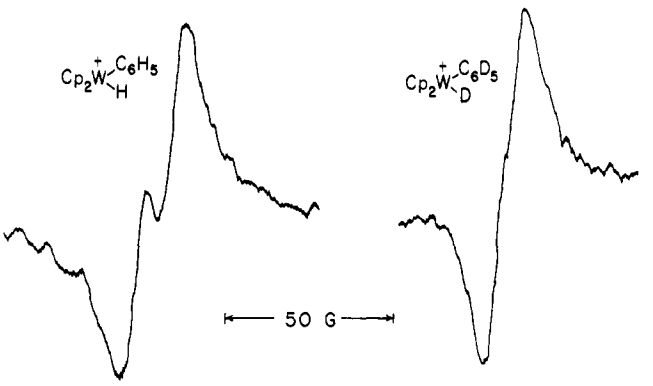

Figure 2. ESR spectra obtained during the electrolysis of (left) $Cp_2W(C_6H_5)H$ and (right) $Cp_2W(C_6D_5)D$ in acetonitrile at −45 °C.

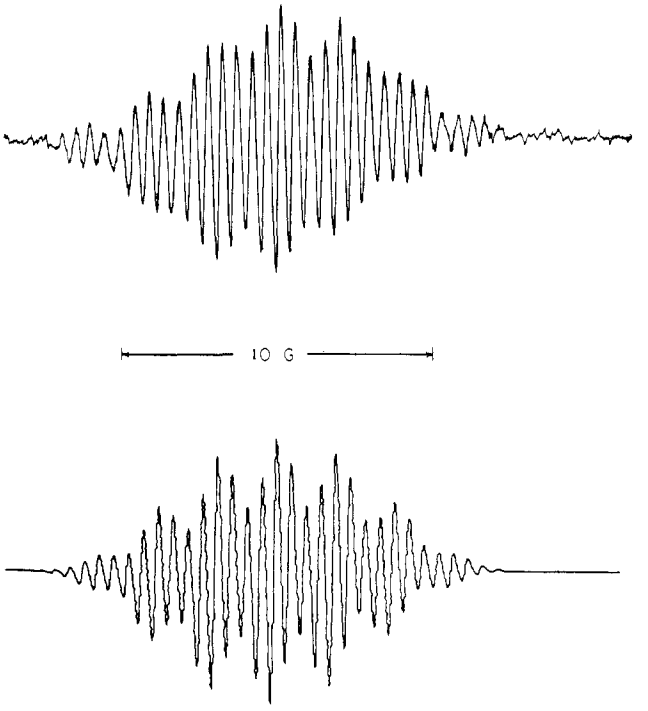

Figure 3. Upper: ESR spectrum obtained in the electrolysis of Cp_2WH_2 with added phenanthroquinone. Lower: computer simulation with the parameters in Table II.

Table II. ESR Coupling Constants for the Spin Adducts to Phenanthroquinone[a]

radical	a(M)	a(H)[c]	a(H′)[d]	a(H″)[d]	a(M)/μ(M)[e]
Cp_2WH·	1.82	3.82	1.90	0.44	16
$Mn(CO)_4$·[b]	5.50		1.72	0.40	1.6
$SnMe_3$·[b]	8.75 (^{119}Sn)		1.87	0.43	13
	8.36 (^{117}Sn)				8.4

[a] In acetone solution at 25 °C. [b] Data taken from ref 7. [c] Coupling due to the metal hydride ligand. [d] Coupling due to the two sets of four equivalent hydrogens on PQ. [e] Ratio of the metal coupling constant to the magnetic moment of the metal.

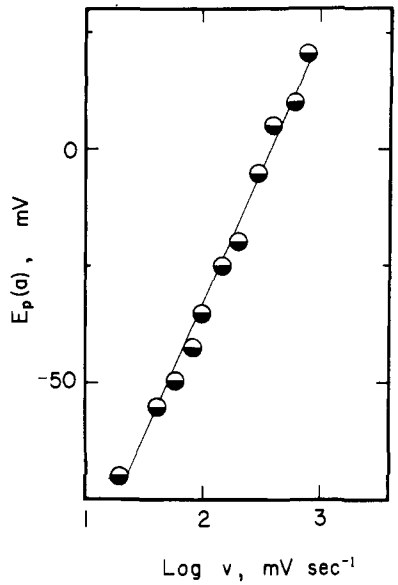

Figure 4. Dependence of the anodic peak potential $E_p(a)$ with sweep rate (log v) during the cyclic voltammetry of Cp_2WH_2 in acetonitrile.

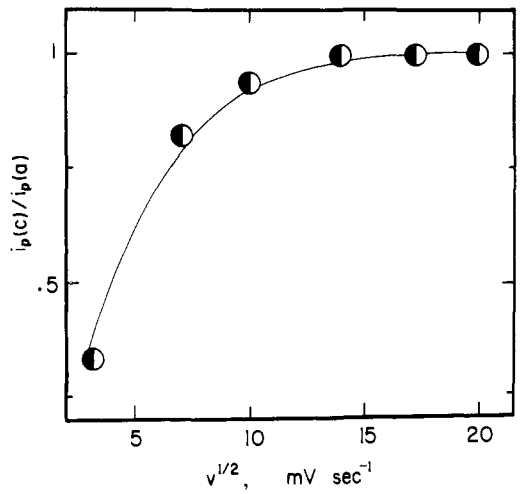

Figure 5. Relationship between the cathodic and anodic current ratio $i_p(c)/i_p(a)$ and the sweep rate ($v^{1/2}$) during the anodic oxidation of $Cp_2W(Ph)H$ at 25 °C.

persistent than $Cp_2WH_2^+$ to allow the cyclic voltammogram to show reversible character at high sweep rates, i.e., $i_p(c)/i_p(a) = 1.01$ at $v \geq 300$ mV s^{-1}. From the decreasing trend in this ratio with v shown in Figure 5, we estimate the half-life of $Cp_2W(Ph)H^+$ to be 20 s. On the other hand, the radical cations derived by anodic oxidation of the dimethyl and dichloro analogues $Cp_2W(CH_3)_2$ and Cp_2WCl_2 are quite persistent. Thus the ESR spectra of both $Cp_2W(CH_3)_2^+$ and $Cp_2WCl_2^+$ following bulk electrolysis show no perceptible change after 1 day. Overall, there is no apparent trend in Table III between the persistence of these tungsten(III) species and the electron density on the metal as indicated by the value of $E_p(a)$. The origin of the lability of the hydrido ligand in both $Cp_2W(Ph)H^+$ and $Cp_2WH_2^+$ is noted in the next section.

C. Radical Cations of Transition-Metal Hydrides as Proton Sources. When $Cp_2W(Ph)H$ is electrolyzed in acetonitrile solution, 0.91 ± 0.05 equiv of hydrogen ion per mol of tungsten is liberated (see Experimental Section). Under similar conditions, Cp_2WH_2 afforded only 0.60 ± 0.05 equiv of $[H^+]$. In both cases, it appears that the hydrogen ion is spontaneously liberated in the course of decomposition of the radical cation, e.g.

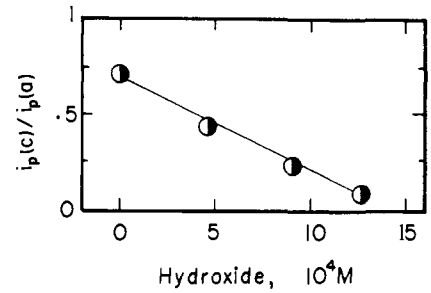

Figure 6. Effect of pH on the peak current ratio of the cathodic and anodic waves in the cyclic voltammogram of $Cp_2W(Ph)H$ in acetonitrile at 25 °C.

Table III. Comparison of the Lifetimes of Radical Cations Derived from Tungstenocene(IV) Analogues at 25 °C

Cp_2WX_2	$E_p(a)$	E^0	τ	g^d
$Cp_2W(CH_3)_2$	−0.395	−0.424	>24 h[a]	2.04
$Cp_2W(Ph)H$	−0.060	−0.090	20 s[b]	2.07
Cp_2WH_2	−0.020	−0.350	$<10^{-3}$ s[c]	
Cp_2WCl_2	+0.394	+0.364	>24 h[a]	1.95

[a] From the decay of the ESR signal. [b] Estimated from the dependence of $i_p(c)/i_p(a)$ on sweep rate on the cyclic voltammogram. [c] From double step chronoamperometry. [d] Isotropic g value.

$$Cp_2WH_2^+ \rightarrow Cp_2WH + H^+ \quad (3)$$

The facile acid dissociation of radical cations of transition-metal hydrides can be shown in another way. Thus the cyclic voltammetry of the tantalum hydride $(dmpe)_2(CO)_2TaH$, where dmpe is bis(dimethylphosphino)ethane, exhibits a reversible oxidative couple at −0.688 V vs. SCE and a second irreversible anodic wave at +0.110 V in Table I. Constant-potential electrolysis at −0.400 and +0.400 V yields 0.94 and 1.01 electron per tantalum, respectively. Thus, $(dmpe)_2(CO)_2TaH^+$ is thermally stable on the CV time scale, and it can be further oxidized in a second (irreversible) step leading to an unstable dication. The addition of a base, n-$Bu_4N^+OH^-$, causes a drastic change in the cyclic voltammogram in which the first anodic wave becomes irreversible and the peak current $i_p(a)$ increases by a factor of 2. Additional base causes no further increase. Since the shift in the peak potential is only 10 mV, we interpret the effect of base as deprotonation of the radical cation to produce a new species which is further oxidized at this potential. Tetrabutylammonium hydroxide does not react with $(dmpe)_2(CO)_2TaH$ under these conditions.

A similar effect of base is noted on the cyclic voltammogram of $Cp_2W(Ph)H$. As the solution is made more basic, Figure 6 shows that only the cathodic wave decreases linearly with the concentration of $[n\text{-}Bu_4N^+\ OH^-]$ due to depletion of $Cp_2W(Ph)H^+$ at the electrode. Since the anodic current $i_p(a)$ remains more or less constant under these conditions, the deprotonated Cp_2WPh is presumably not oxidized at this potential.

III. Products Derived from Paramagnetic Transition-Metal Hydrides. Controlled-potential electrolysis coupled with coulometry of transition-metal hydrides also allows the products of the radical cations to be isolated and characterized. We have identified at least three processes associated with the decomposition of these paramagnetic transition-metal hydride cations as (1) oxidative-coupling, (2) addition, and (3) reductive elimination as described individually below.

A. Oxidative Coupling of $CpMo(CO)_3H$. Controlled-potential electrolysis of $CpMo(CO)_3H$ in acetonitrile at 0.50 V vs. SCE required 1.08 ± 0.05 electrons per molybdenum. The product was isolated by precipitation with water and identified as the dimer $[CpMo(CO)_3]_2$ by comparison of its IR and ^1H NMR

Table IV. Fractional Atomic Coordinates[a]

atom	10^4x	10^4y	10^4z	$10B_{iso}$
W(1)	1404.6(4)	3050.2(4)	7858.9(7)	17
W(2)	3869.4(4)	3196.9(5)	10321.3(7)	19
CL(1)	2419(3)	1706(3)	3663(5)	21
C(1)	1881(11)	1438(11)	8301(21)	23
C(2)	1392(16)	1607(14)	8879(22)	38
C(3)	461(13)	1873(14)	7570(20)	27
C(4)	477(14)	1867(14)	6313(20)	30
C(5)	1354(15)	1635(13)	6762(23)	31
C(6)	1720(13)	4643(12)	8696(24)	34
C(7)	1251(19)	4640(14)	7175(33)	51
C(8)	365(12)	4177(12)	6440(20)	27
C(9)	335(12)	3993(13)	7606(22)	30
C(10)	1153(17)	4223(14)	8990(26)	44
C(11)	3488(12)	2850(15)	7950(20)	29
C(12)	4057(18)	2116(13)	8951(25)	37
C(13)	4891(12)	2564(14)	10078(21)	28
C(14)	4862(13)	3529(15)	9797(23)	30
C(15)	3990(15)	3742(17)	8550(19)	38
C(16)	3456(11)	3102(12)	11936(21)	24
C(17)	4056(14)	2336(13)	12199(20)	33
C(18)	4887(14)	2726(20)	12659(22)	43
C(19)	4871(12)	3685(17)	12687(18)	30
C(20)	4030(16)	3884(16)	2320(23)	39
C(21)	2740(11)	−412(11)	6523(19)	25
C(22)	3233(13)	4427(12)	4710(20)	26
C(23)	1573(14)	4415(18)	3771(24)	41
O(1)	2137(12)	1747(11)	4555(19)	42
O(2)	2037(8)	2479(9)	2657(14)	30
O(3)	2134(12)	787(10)	2874(19)	53
O(4)	3390(10)	1756(13)	4602(20)	51
O(5)	2004(10)	4931(12)	2253(15)	42

[a] Estimated standard deviations of the least significant figure(s) are given in parentheses in this and all subsequent tables.

spectra with those of an authentic sample.[9] We conclude that the stoichiometry accompanying electrolysis is

$$2CpMo(CO)_3H - 2e \rightarrow [CpMo(CO)_3]_2 + 2H^+ \quad (4)$$

B. Additive Dimerization of Cp_2WH_2. When a colorless solution of Cp_2WH_2 in acetonitrile was electrolyzed at a controlled potential of −0.20 V at 0 and −78 °C, it produced an intense violet solution absorbing at λ_{max} 545 nm. Workup of the electrolysate afforded dark purple crystals of a dimeric tungstenocene hydride salt, $(Cp_2W)_2H_3^+ ClO_4^-$, which we characterized by X-ray crystallography, as described in the following section. The ^1H NMR spectrum of the dimeric salt in acetone-d_6 solution showed a single sharp resonance at δ 5.37 ppm for the cyclopentadienyl ligands and a single hydride resonance at δ −16.20 ppm in the ratio of 20 "Cp" to 2.9 "H". The IR spectrum of the solid taken in Nujol exhibits a strong, sharp band at 2030 cm^{-1} which is 180 cm^{-1} higher in frequency than that observed in the parent Cp_2WH_2, and it is clearly in the region expected for terminal hydrides.[10]

The cyclic voltammogram of the dimeric ion, $(Cp_2W)_2H_3^+$, shows three anodic waves at +0.480, +0.665, and +0.870 V and one cathodic wave at −1.390 V vs. SCE. All four waves are totally irreversible, but, after passing through the cathodic wave, an anodic sweep reveals the presence of a new species with $E_p(a) = -0.020$ V which is the same as that of Cp_2WH_2. We infer that electron transfer to the dimer cation is accompanied by reductive fragmentation, i.e.

$$(Cp_2W)_2H_3^+ + e \rightarrow Cp_2WH_2, \text{ etc.} \quad (5)$$

Since the four waves observed in the CV of $(Cp_2W)_2H_3^+$ are identical with all the secondary waves observed in the voltammogram of Cp_2WH_2 taken at room temperature, we conclude that the dimer cation is the principal, if not the sole, species produced upon the oxidation of Cp_2WH_2 according to the stoichiometry

$$2Cp_2WH_2 \xrightarrow{-2e} (Cp_2W)_2H_3^+ + H^+ \quad (6)$$

C. Reductive Elimination from $Cp_2W(Ph)H^+$. Controlled-potential electrolysis of an acetonitrile solution of $Cp_2W(Ph)H$ at +0.20 V yields 0.96 ± 0.05 electrons per tungsten. In the course of electrolysis, the solutions darkens and deposits a brown, amorphous precipitate. Careful vacuum distillation of all the volatile material directly from the electrolysate afforded an acetonitrile solution containing 0.94 ± 0.05 mol of benzene per tungsten charged (see Experimental Section). The resultant brown residue was extracted with water to remove the supporting electrolyte and soluble salts. Titration of the aqueous extract with alkali indicated the presence of 0.91 ± 0.05 equiv of acid per tungsten. The partial stoichiometry is

$$Cp_2W(Ph)H \xrightarrow{-e} C_6H_6 + H^+, \text{ etc.} \quad (7)$$

In order to examine the origin of the benzene, an acetonitrile solution of the perdeuterio derivative $Cp_2W(C_6D_5)D$ was oxidized as +0.20 V under the same conditions. Analysis by GC–MS allowed the benzene fraction to be identified as predominantly the monoprotio derivative C_6D_5H, as described in the Experimental Section.

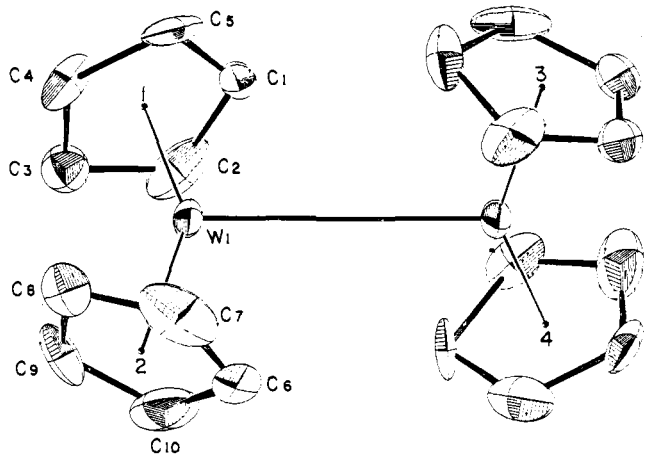

Figure 7. ORTEP drawing of the tungstenocene hydride dimer, $(Cp_2W)_2H_3^+ClO_4^-(CH_3)_2CO$, showing the numbering scheme of atoms. Carbon (C3) has been assigned an isotropic thermal parameter, and all atoms are drawn at the 50% probability level.

IV. Crystal Structure of $(Cp_2W)_2H_3^+ClO_4^-$. Crystals of the dimer cation $(Cp_2W)_2H_3^+ClO_4^-$ are extremely air sensitive and highly susceptible to the thermal loss of acetone of crystallization. These bothersome properties caused extraordinary difficulties in growing and mounting crystals suitable for X-ray crystallography (see Experimental Section), and precluded any further attempt for a neutron diffraction determination of the structure. The nonhydrogen atoms in the X-ray crystal structure of $(Cp_2W)_2H_3^+ClO_4^-$ are located in Table IV, which defines the fractional atomic coordinates, and they are shown in Figure 7 containing an ORTEP view with an atom numbering scheme. The important bond distances and angles are presented in Tables V and VI, respectively.

Although it is not required by the space group, the molecule has refined to a C_2 symmetry in the crystal, in which the planes defining the Cp_1–W_1–Cp_2 and Cp_3–W_2–Cp_4 units are nearly perpendicular to each other. More importantly, there are significant deviations from an idealized staggered arrangement of Cp–W–Cp units about the W–W bond. Thus the W–W bond does not lie in either of the planes defined by Cp_1–W_1–Cp_2 or Cp_3–W_2–Cp_4, but forms an angle of $\theta = 159°$ to

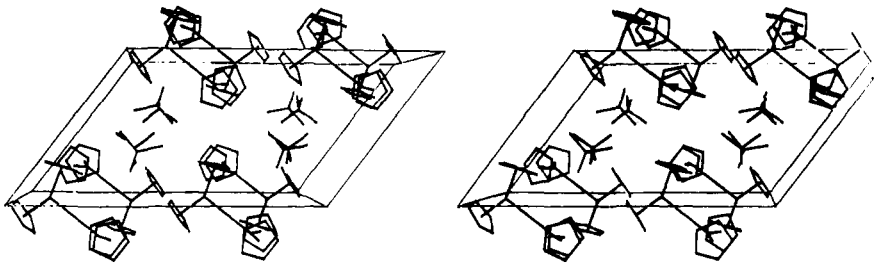

Figure 8. Stereoscopic ORTEP packing diagram for $(Cp_2W)_2H_3^+ClO_4^-(CH_3)_2CO$.

Table V. Selected Bond Distances[a]

A	B	distance, Å
W(1)	W(2)	3.628(1)
W(1)	C(1)	2.345(15)
W(1)	C(2)	2.316(18)
W(1)	C(3)	2.260(19)
W(1)	C(4)	2.250(17)
W(1)	C(5)	2.292(16)
C(1)	C(2)	1.410(30)
C(1)	C(5)	1.411(28)
C(2)	C(3)	1.485(29)
C(3)	C(4)	1.430(21)
C(4)	C(5)	1.408(31)
W(1)	Cp(1)	1.945
W(2)	Cp(2)	1.939
W(2)	Cp(3)	1.955
W(2)	Cp(4)	1.948

[a] All four Cp rings are the same to within experimental error. The Cp distances in the last four entries are given to the centroid.

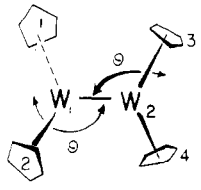

each. The stereoscopic perspective of the unit cell shown in Figure 8 indicates that such a distortion is unlikely to arise from packing forces. Another noteworthy feature of the crystal structure is the W-W distance of 3.628 Å, which is 0.4 Å longer than the single bond length of 3.222 Å reported for $Cp_2W_2(CO)_6$.[11] We believe that both the apparent distortion and the unusual bond length can be used to deduce the location of the three hydrido ligands as presented in the Discussion.

Discussion

Electrochemical studies show that transition-metal hydrides are excellent electron donors, undergoing one-electron oxidation at relatively low electrode potentials.

I. Formation and Decomposition of Paramagnetic Transition-Metal Hydrides. The paramagnetic radical cations derived from the diamagnetic transition-metal hydrides in Table I are characteristically all labile species. The most stable of these, $(dmpe)_2(CO)_2TaH^+$, can be easily observed directly by ESR spectroscopy, and it persists for less than 1 min in solution. However, the detection of the others, such as $Cp_2W(Ph)H^+$, depends on cyclic voltammetry at high sweep rates. Finally, evidence for the highly labile $Cp_2WH_2^+$ is only obtained by ac polarography owing to its half-life of less than 1 ms.

We attribute the transitory character of these paramagnetic radical cations to the facile loss of a proton to generate a neutral, paramagnetic species, i.e.

Table VI. Selected Bond Angles

A	B	C	angle, deg
Cp(1)[a]	W(1)	Cp(2)	145.6
Cp(3)	W(2)	Cp(4)	143.8
W(2)	W(1)	Cp(1)	106.0
W(2)	W(1)	Cp(2)	106.2
W(1)	W(2)	Cp(3)	105.7
W(1)	W(2)	Cp(4)	107.7

[a] Calculated as the geometric center of the cyclopentadiene ring.

$$MH \xrightarrow[(a)]{-e} MH^+\cdot \xrightarrow[(b)]{fast} M\cdot + H^+, \text{ etc.} \qquad (8)$$

In some of the examples listed in Table I, proton loss in step b may even be faster than electron transfer in step a, and no evidence for electrochemical reversibility is observed, either by cyclic voltammetry or ac polarography. The extreme lability of the radical cations of these metal hydrides is in contrast to the relatively more stable alkyl and halo analogues, such as $Cp_2W(CH_3)_2^+$ and $Cp_2WCl_2^+$.

Reversible deprotonation of diamagnetic metal hydrides is well known.[12] Although an increase in the positive charge on the metal center as a result of oxidation should facilitate this process, electronic factors must also be considered. Thus, the electrochemistry of Cp_2WH_2 at low temperatures indicates that acid dissociation from the radical cation is complete in acetonitrile solutions containing only tetraethylammonium perchlorate as supporting electrolyte, i.e.

$$Cp_2WH_2^+ClO_4^- \underset{CH_3CN}{\overset{K}{\rightleftharpoons}} Cp_2WH + H^+ClO_4^- \qquad (9)$$

where $K \gg 1$. In marked contrast, the analogous equilibrium for the diamagnetic trihydride cation, i.e.

$$Cp_2WH_3^+ \overset{K'}{\rightleftharpoons} Cp_2WH_2 + H^+ \qquad (10)$$

lies to the left ($K' \ll 1$), since Cp_2WH_2 is readily protonated even at low acidities.[13]

Subsequent to deprotonation, the resultant metal-centered radicals may combine to form a new metal-metal bond. Such a dimerization is known to be a facile process for the cyclopentadienyldicarbonylmolybdenum(I) radical.[14] The overall process for the oxidative coupling of $CpMo(CO)_3H$ is then represented as in Scheme I.

Scheme I

$$CpMo(CO)_3H \overset{-e}{\rightleftharpoons} CpMo(CO)_3H^+ \qquad (11)$$

$$CpMo(CO)_3H^+ \rightarrow CpMo(CO)_3 + H^+ \qquad (12)$$

$$2CpMo(CO)_3 \rightarrow Cp_2Mo_2(CO)_6 \qquad (13)$$

In a similar manner, the formation of the dimer cation during the oxidation of Cp_2WH_2 may be formulated as a coupling of tungsten-centered radicals, i.e., Scheme II.

Scheme II

$$Cp_2WH_2 \overset{-e}{\rightleftharpoons} Cp_2WH_2^+ \quad (14)$$

$$Cp_2WH_2^+ \rightarrow Cp_2WH + H^+ \quad (15)$$

$$2Cp_2WH \rightarrow Cp_4W_2H_2 \quad (16)$$

$$Cp_4W_2H_2 + H^+ \rightarrow Cp_2W_2H_3^+ \quad (17)$$

Indeed, the neutral radical Cp_2WH can be trapped with phenanthroquinone as the PQ adduct in eq 2, prior to coupling in eq 16. However, attempts to trap Cp_2WH with organic halides such as bromobenzene and methyl iodide or with diphenylacetylene, cyclohexene, carbon dioxide, and carbon monoxide were unsuccessful. The short lifetime of Cp_2WH suggests that a bimolecular coupling such as eq 16 may not be the route for dimer formation. Instead, it may arise from an addition to Cp_2WH_2, followed by electron transfer, i.e.

$$Cp_2WH + Cp_2WH_2 \rightarrow Cp_4W_2H_3 \quad (18)$$

$$Cp_4W_2H_3 \overset{-e}{\rightarrow} Cp_4W_2H_3^+ \quad (19)$$

Unfortunately, the short life of Cp_2WH does not allow its concentration to be measured and a kinetic distinction to be made between these mechanisms.

Paramagnetic species derived from the oxidation of metal hydrides may also undergo reductive elimination as shown by the formation of benzene in high yield from $Cp_2W(Ph)H$. Deuterium-labeling studies show, however, that benzene probably does not arise from a direct process such as eq 20.

$$Cp_2\overset{+}{W}\begin{matrix} \diagup C_6D_5 \\ \diagdown D \end{matrix} \rightarrow C_6D_6 + Cp_2W^+ \quad (20)$$

Instead the hydrogen must be derived either from the solvent (CH_3CN) or the ligand (Cp) since it is predominantly labeled as C_6D_5H (see Experimental Section). In either case, the neutral Cp_2WPh formed by deprotonation of the radical cation is the likely precursor, and this coordinatively unsaturated 17-electron species may eject a phenyl radical followed by hydrogen atom abstraction from solvent, e.g.

$$Cp_2WC_6D_5 \rightarrow Cp_2W + C_6D_5\cdot \quad (21)$$

$$C_6D_5\cdot + CH_3CN \rightarrow C_6D_5H + \cdot CH_2CN, \text{ etc.} \quad (22)$$

Alternatively, it may undergo a direct intramolecular elimination of benzene by removal of a hydrogen on the cyclopentadienyl ligand, i.e.

$$Cp_2WC_6D_5 \rightarrow C_6D_5H + CpWC_5H_4, \text{ etc.} \quad (23)$$

Such a mode of elimination is known for the reduction of $Cp_2Ti(CH_3)_2$ and the decomposition of Cp_3ThBu and Cp_3UMe.[15-17] Moreover, the intractable tungsten-containing product, possibly derived from $CpWC_5H_4$ in eq 23, is reminiscent of bridging C_5H_4 units present as μ-(η^5:η^1-fulvalene) ligands in the related titanium, thorium, and uranium analogues.

II. Molecular Structure of the Tungstenocene Hydride Dimer Cation. The ^1H NMR and IR spectra of $(Cp_2W)_2H_3^+$ indicate the presence of three hydride ligands, some of which are terminally bonded to tungsten.[18] Furthermore, the long W-W bond of 3.628 Å in the crystal structure of $(Cp_2W)_2H_3^+$ suggests the presence of a bridging hydrogen. If so, it is longer than any of the W-W distances in dinuclear tungsten hydrides known from neutron diffraction studies to contain the W-H-W bridging unit, viz., 3.328 Å in α-$HW_2(CO)_9(NO)$,[19] 3.330 Å in β-$HW_2(CO)_9(NO)$,[19] 3.340 Å in $HW_2(CO)_{10}^-PPh_4^+$,[20] 3.393 Å in $HW_2(CO)_8(NO)P(OMe)_3$,[21] and 3.528 Å in $HW_2(CO)_{10}^-NEt_4^+$.[20] The W-W distances in the latter increase with the W-H-W bond angles, while the W-H bond length remains relatively constant at 1.88 Å. Using this value, an upper limit of 3.8 Å may be estimated for the W-W distance in a linear W-H-W configuration. Therefore, while the W-W distance in $(Cp_2W)_2H_3^+$ is the longest known for a tungsten dimer with bridging hydrogen, it is still 0.1-0.2 Å shorter than that expected for a linear W-H-W unit.

Table VII. Least-Squares Fit of Cp_2MoH_2 to $Cp_4W_2H_3^+$

atom A	atom B	Δd,[a] Å
Mo(1)	W(1)	0.139
Cp(1)	Cp(2)	0.037
Cp(1)′	Cp(1)	0.031
C(4)	C(6)	0.119
C(5)	C(10)	0.092
C(1)	C(9)	0.119
C(2)	C(8)	0.199
C(3)	C(7)	0.076
C(3)′	C(1)	0.139
C(4)′	C(5)	0.124
C(5)′	C(4)	0.180
C(1)′	C(3)	0.122
C(2)′	C(2)	0.128
W(2)	Mo(1)	0.158
Cp(3)	Cp(1)	0.034
Cp(4)	Cp(1)′	0.032
C(11)	C(4)	0.102
C(12)	C(5)	0.088
C(13)	C(1)	0.092
C(14)	C(2)	0.124
C(15)	C(3)	0.116
C(16)	C(3)′	0.105
C(20)	C(4)′	0.133
C(19)	C(5)′	0.185
C(18)	C(1)′	0.109
C(17)	C(2)′	0.079

[a] Deviation from perfect fit of Cp_2W and Cp_2Mo; see Experimental Section for details.

In order to place the remaining pair of hydridic ligands, we note the very strong similarity between the structure of the Cp_2W units in $(Cp_2W)_2H_3^+$ and the structure of the Cp_2Mo unit in Cp_2MoH_2 shown below, which was recently established

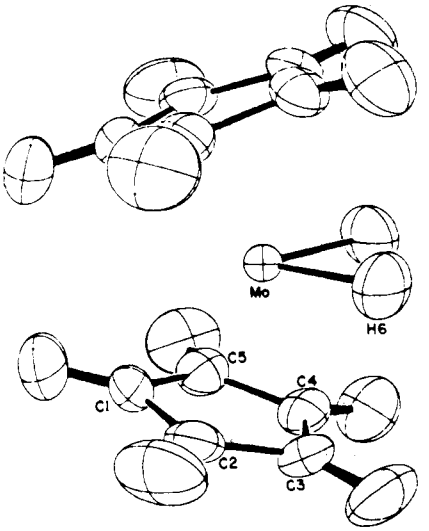

in a high-precision neutron-diffraction determination.[22] Indeed, the excellent least-squares fit resulting from the superposition of a Cp_2Mo unit onto each half of the $(Cp_2W)_2H_3^+$ dimer presented in Table VII indicates that both metallocene units are virtually identical. [Strictly speaking, the Cp_2W units in Cp_2WH_2 should be employed in such a comparison. However, the structure of Cp_2WH_2 is unavailable, and we used the

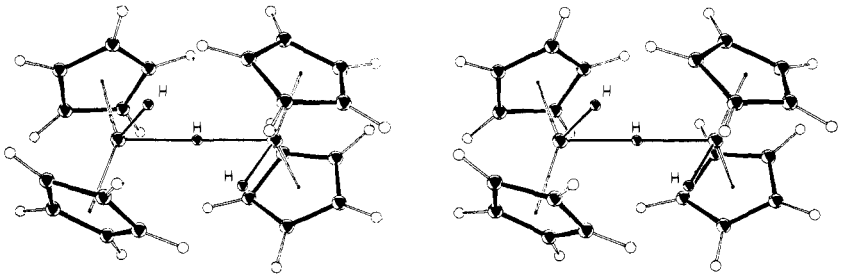

Figure 9. Stereoscopic view of the molecular structure of tungstenocene hydride dimer $(Cp_2W)_2H_3^+$ showing the location of the hydrido ligands deduced by the least-squares fit of Cp_2MoH_2. Carbon C(3) has been given an artificial isotropic thermal parameter and all hydrogens are drawn assuming $B_{iso} = 0.5$. Thermal ellipsoids are drawn at the 50% probability level.

structure of Cp_2MoH_2 since the atomic parameters of tungsten and molybdenum (due to the lanthanide contraction) are known to be very similar.[23]] Thus, exchanging a terminal hydride with a bridging hydride has no structural effect on the metallocene core. More significantly, the high degree of overlap between the monomeric Cp_2MoH_2 units and the $(Cp_2W)_2H_3^+$ dimers argues against steric repulsion between the cyclopentadienyl rings as the primary reason for the long W–W distance. Indeed, the independent superposition of a Cp_2MoH_2 molecule onto each half of $(Cp_2W)H_3^+$ by least-squares refinement yields four hydrogen positions, two bridging and two terminal. The two bridging hydrogens lie on the same side of the W–W axis, and are sufficiently close to each other (0.8 Å) to be reasonably averaged as a single position to compute a W–H bridge distance of 1.9 Å. The perspective view of the molecular structure of $(Cp_2W)_2H_3^+$ deduced in this manner is shown in Figure 9. The location of the three hydride ligands in $(Cp_2W)_2H_3^+$ results in nonbonded contacts listed in Table VIII, which are nearly the same as those reported for Cp_2MoH_2. These locations are completely consistent with the minimum nonbonding contacts determined from neutron-diffraction analyses.[25] The latter lends further support for the assumption that no unusually large steric repulsions exist between the metal centers in $(Cp_2W)_2H_3^+$ to account for an otherwise long W–W distance.

The presence of a bridging hydride proposed for $(Cp_2W)_2H_3^+$ can also qualitatively account for its unusual absorption at λ_{max} 545 nm, since neither monomeric Cp_2WH_2 nor Cp_2MoH_2 exhibits any electronic transitions in the visible region of the spectrum.[26] According to a simple MO energy diagram below, the principal difference between a terminal

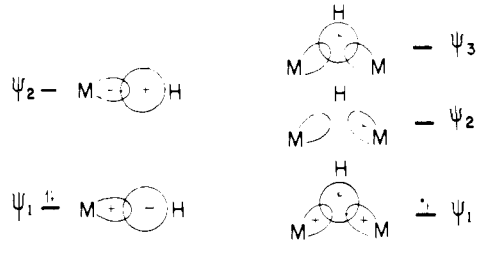

and bridging hydride is the presence of an empty low-lying orbital Ψ_2 in the latter, which is antibonding with respect to the M–M bond. While transitions in the bridged system must occur at lower energies compared to the terminal hydride, detailed spectral interpretations cannot be made at this juncture since the ground state cannot be assigned with any degree of confidence.[27-29] The cyclic voltammetric results are also consistent with this simple MO formulation. Thus, $(Cp_2W)_2H_3^+$ is reduced irreversibly at −1.39 V vs. SCE. The presence of Cp_2WH_2 in the reverse anodic sweep indicates that the $(Cp_2W)_2H_3$ is unstable relative to the rupture of the dimeric unit. In contrast, the monomer Cp_2WH_2 is much less susceptible to reduction, showing no cathodic wave out to −2.0 V.

Table VIII. Comparison of the Shortest Nonbonded Hydrogen Contacts Observed for Cp_2MoH_2[a] with Those for the Proposed Location in $Cp_4W_2H_3^+$

A type of atom	B type of atom	Cp_2MoH_2, Å	$Cp_4W_2H_3^+$, Å
	Intramolecular Contacts		
hydride	hydride	2.063	2.023
ring (carbon)	hydride	2.368	2.347
ring (hydrogen)	hydride	2.455	1.829
ring (hydrogen)	ring (hydrogen)	2.454	2.296
metal	hydride	not applicable	1.861
	Intermolecular Contacts		
ring (hydrogen)	ring (hydrogen)	2.310	2.402
ring (hydrogen)	hydride	2.479	>3.00

[a] Based on the data from ref 21.

Experimental Section

Materials. Cp_2WH_2, $Cp_2W(C_6H_5)H$, and $CpMo(CO)_3H$ were prepared according to published procedures.[9,30] $Cp_2W(C_6D_5)D$ was prepared in a similar manner,[31] by the photolysis of Cp_2WH_2 (0.20 g, 0.63 mmol) in 5 mL of C_6D_6 for 12 h using a low-pressure mercury lamp. The ^1H NMR spectrum of the product showed only a singlet resonance at δ 4.59 due to Cp, and the high-field region of the spectrum was devoid of any hydride resonances. $IrH(CO)(PPh_3)_3$ was purchased from Strem Chemical Co., $RhH(CO)(PPh_3)_3$ was a gift from H. B. Copelin, and $RhH(PPh_3)_4$ and $TaH(PMe_2CH_2CH_2PMe_2)_2(CO)_2$ were gifts from U. Klabunde. $FeH_2(PPh_2CH_2CH_2PPh_2)_2$ was prepared by K. Rollick according to a published procedure.[32] Reagent grade acetonitrile was further purified by refluxing over calcium hydride, treated with potassium permanganate, and redistilled from P_2O_5 through a 19-plate bubble cap Oldershaw column. Solvents were stored under argon in Schlenk flasks. Tetraethylammonium perchlorate (TEAP) was obtained from G. F. Smith Chemical Co. and used without further purification.

Electrochemical Measurements. Electrochemistry was performed on a Princeton Applied Research Model 173 potentiostat equipped with a Model 176 current-to-voltage converter which provided a feedback compensation for ohmic drop between the working and reference electrodes. The voltage follower amplifier (PAR Model 178) was mounted external to the main potentiostat with a minimum length of high impedance connection to the reference electrode (for low noise pickup). Cyclic voltammograms were recorded on a Houston Series 2000 X-Y recorder. Phase angle measurements were made with a Princeton Applied Research Model 5203 lock-in amplifier. The electrochemical cell was constructed according to the design of Duyne and Reilley.[33] The distance between the platinum working electrode and the tip of the salt bridge was 1 mm to minimize ohmic drop. Bulk coulometry was carried out in a three-compartment cell of conventional design with a platinum gauze electrode. Complete electrolysis of 0.2 mmol of electroactive material generally required 5–10 min, and was graphically recorded on a Leeds and Northrup Speedomax strip chart recorder. The current–time curve was manually integrated.

Isolation of Products. $Cp_2Mo_2(CO)_6$. A solution of $CpMo(CO)_3H$ (95 mg) in 8 mL of acetonitrile containing 0.1 M tetraethylammonium perchlorate was electrolyzed at 0.50 V vs. SCE. The electrolysis was continued for 5 half-lives in the exponential decay of the current. The

measured area was 37.2 A s, which yields 1.08 ± 0.05 electrons/mol Mo. A large excess (200 mL) of deaerated water was added to the anolyte, and the resultant red microcrystals were filtered, washed with water, and dried in vacuo, yield 57 mg (60%).

$(Cp_2W)_2H_3^+ClO_4^-$. The electrolysis cell was charged with 0.464 g of Cp_2WH_2 and 10 mL of acetonitrile which was 0.1 M in tetraethylammonium perchlorate. Initially the Cp_2WH_2 was only partially dissolved, but, as the solution was electrolyzed at 0 °C and +0.200 V, the yellow solid dissolved and the solution became deep violet. The measured area of the current-time curve was 114 A s, which yields 0.80 ± 0.05 electrons/mol W. The acetonitrile was removed in vacuo at 0 °C from the anolyte. The resultant violet solid was washed with three 20-mL portions of degassed water to remove the supporting electrolyte. The violet solid was again dried in vacuo and recrystallized at −78 °C from acetone, yield 0.31 g (67%). Neutralization of the brown aqueous washings with aqueous KOH yielded a small amount of Cp_2WH_2. Thus, the low value of electrons per mol of tungsten is due to the formation of the electroinactive $Cp_2WH_3^+$ ion from the acid produced during electrolysis.

The ^1H NMR and IR spectra of $(Cp_2W)_2H_3^+$ were of limited value in making assignments of the hydrido ligand. Similar examples are extant. Thus, the molecular structure of $[Cp_2ThH_2]_2$ has been determined by neutron diffraction and shown to contain two terminal and two bridging hydrides. Yet the hydride resonance at δ 19.25 in toluene-d_8 remains a singlet down to −90 °C,[34] indicating a rapid bridge-terminal exchange process which may be quite general for (H)M-H-M(H) systems. Similarly, terminal M-H stretching modes of transition-metal hydrides are readily identified as IR absorptions at 1900 ± 300 cm^{-1}, with intensities that usually are stronger than C-H stretching modes.[10a] In contrast, the M-H modes of hydride-bridged metal complexes are frequently weak and broad in both the IR and Raman spectra. Furthermore, they occur at significantly lower frequencies, 1200–1800 cm^{-1}. Thus, the symmetric stretch in $(Et_4N)[HW_2(CO)_{10}]$ at 1683 cm^{-1} can only be resolved below 150 K.[10b]

Anodic Oxidation of $Cp_2W(Ph)H$. A Sargent Model S-30072-15 glass membrane pH electrode was placed into the anodic compartment of the electrolysis cell which contained 10 mL of a 1.8×10^{-2} M solution of $Cp_2W(Ph)H$ in acetonitrile with 0.1 M tetraethylammonium perchlorate. The offset of the pH meter was adjusted to read 7.0. The solution was oxidized with a platinum gauze electrode at +0.20 V vs. SCE. When the electrolytic current dropped to zero, the reading of the pH meter was 3.1.[35] In an alternative experiment, a solution containing 156 mg (0.398 mmol) of $Cp_2W(Ph)H$ in 10 mL of acetonitrile with 0.1 M TEAP was oxidized at +0.20 V. Integration of the current yielded 3.68 C or 0.96 ± 0.05 electrons per tungsten. As the electrolysis proceeded, the initially yellow solution darkened and deposited a brown precipitate. The solvent was removed in vacuo and analyzed by gas chromatography on a 15-ft Apiezon L column at 150 °C using a toluene internal standard and found to contain 0.345 mmol or 0.94 ± 0.05 equiv of benzene per tungsten. The resultant brown tungsten residuals were extracted with water to remove the supporting electrolyte and acid. The water washings were titrated with 0.0590 M standard NaOH solution to a phenolphthalein end point, yielding 0.362 mmol or 0.91 ± 0.05 equiv of hydrogen ion per tungsten.

Electrolysis of $Cp_2W(D)(C_6D_5)$. An acetonitrile solution of 27 mg (0.069 mmol) of $Cp_2W(D)C_6D_5$ in 8.0 mL of CH_3CN with 0.1 M TEAP was electrolyzed at +0.05 V vs. SCE. The solvent was removed from the supporting electrolyte and tungsten product in vacuo, and the distillate analyzed by a Hewlett-Packard 5992 GC-MS system. A 20-ft OV-17 column operating at 80 °C was employed. Samples of C_6D_6 and C_6H_6 diluted to similar concentrations in acetonitrile were also run at the same time to determine the mass spectral cracking pattern. There were only four statistically significant peaks in the sample from the oxidation, viz., *m/e* (intensity) 84 (28), 83 (100), 82 (21), and 81 (16). The GC-MS of C_6H_6 under the same conditions afforded *m/e* (intensity) 79 (6), 78 (100), 77 (22), 76 (5), and 75 (4), and C_6D_6 afforded *m/e* (intensity) 85 (6), 84 (100), 82 (15), 80 (3), and 78 (0). The presence of acetonitrile in the mass spectrum could not be circumvented since it tailed off of several chromatographic columns used and may be responsible for the P + 1 peak from C_6H_6 and C_6D_6. From the analysis of the data, the benzene fraction contained 80 ± 4% C_6D_5H and 20 ± 4% C_6D_6. An uncertainty of ±6% in the magnitude of the *m/e* 84 peak may lead to small amounts of $C_6D_4H_2$.

Oxidation of Cp_2WH_2 in the Presence of Pyridine. Pyridine purified by distillation from $LiAlH_4$ was shown to be electroinactive at 0.00 V vs. SCE. A solution of 89.1 mg (0.282 mmol) of Cp_2WH_2 and 0.06 M pyridine in 10 mL of acetonitrile with 0.1 M TEAP was oxidized at 0.00 V. The acetonitrile and unreacted pyridine were removed in vacuo, and the residual pyridinium perchlorate was extracted with CD_3CN and quantitated by integration of the ^1H NMR resonance (δ 8.70, 8.00, unresolved multiplets) against a methylene chloride internal standard. This analysis yielded 0.017 mmol or 0.60 ± 0.05 $[pyH]^+$ per tungsten. For comparison, an authentic sample of pyridinium perchlorate was prepared by mixing near-saturated aqueous solutions of sodium perchlorate and pyridinium iodide. The resultant solid was filtered, washed with water, and dried in vacuo.

Spin Trapping of Cp_2WH. A solution of 50 mg (0.16 mmol) of Cp_2WH_2 in 10 mL of acetone with 0.1 M TEAP was oxidized at +0.10 V while being cooled to −78 °C. After the electrolytic current had decayed for approximately 4 half-lives (250 s), the cell was disconnected and 50 mg of phenanthroquinone was added. The solution was allowed to warm to room temperature, and the ESR spectrum recorded. A weak signal was observed. The experiment was repeated three times, whereupon it was found that the most intense ESR signal was obtained when the electrolysis was stopped after the current had decayed by about 30% and the phenanthroquinone was added immediately. Control experiments demonstrated that phenanthroquinone did not react with either the reactant Cp_2WH_2 or the product $Cp_4W_2H_3^+$ to yield any paramagnetic species. Thus, when PQ was reacted with an authentic sample of $Cp_4W_2H_3^+$ which had been isolated as described above, no color change or ESR signal was observed. With Cp_2WH_2, however, there is a series of color changes proceeding from orange-brown to purple to dark brown. The identity of the species responsible for these colors is not known. However, no ESR signal could be detected at any stage of this reaction. The visible spectrum of the solution with λ_{max} 4100 Å included in a broad tail extending to 6000 Å does not correspond to that of $Cp_4W_2H_3^+$, λ_{max} 5450 Å.

Ac Polarography of Cp_2WH_2. A 2.5×10^{-2} M solution of Cp_2WH_2 in acetone-acetonitrile (60/40%) mixed solvent which was 0.2 M in tetrabutylammonium perchlorate was examined at a platinum microelectrode with a dc scan rate of 20 mV s^{-1} and a 5-mV peak-to-peak ac modulation over the frequency range of 10–1000 Hz. The temperature was maintained at −77 ± 0.3 °C with a stream of cold nitrogen. The phase shift of the charging current observed in the absence of electrochemical processes was less than 90° and decreased with increasing frequency owing to small uncompensated cell resistance present at this low temperature.[36] The charging current with its associated phase angle was used to empirically measure the net cell resistance, and in conjunction with the equations derived by Elving[37] the data was corrected for the phase error induced by the uncompensated cell resistance. The criteria for a reversible fundamental-harmonic ac polarographic wave[38] were met for frequencies above 250 Hz. The cotangent of the phase angle was observed to be unity and independent of frequency, viz., cot θ (frequency) 1.3 (250 Hz), 0.9 (500 Hz), 0.7 (750 Hz), and 1.1 (1000 Hz). The plot of current vs. $\omega^{1/2}$ was linear with intercept at the origin and the half-width of the ac wave was 80 mV.

X-ray Data Collection and Structure Analysis. Crystals suitable for X-ray analysis were grown by slow cooling of an acetone solution from 0 to −78 °C. The violet crystals are highly unstable, decomposing when allowed to warm above dry ice temperatures or upon exposure to oxygen. A suitable crystal was quickly mounted using silicone grease and transferred to the goniostat, which was equipped with a nitrogen boil-off cooling nozzle at −145 °C. Significant decomposition occurred even though the sample transfer required less than 3–4 s. The crystal dimensions [*hkl*] (distance in cm) follow: [010](0.0168), [0 − 10](0.0168), [100](0.0256), [−100](0.0256), [101](0.007), [−10 − 1](0.007), [0 − 11](0.002). The space group is $P2_1/a$. The lattice constants were calculated by least-squares refinement on the setting angles of 28 reflections yielding a = 18.389 (5) Å, b = 13.886 (4) Å, c = 11.244 (3) Å, β = 126.96 (2)°, V = 2294.31 Å^3. The calculated density with Z = 4 is 2.089 g/cm^3.

Intensity data were collected by the $\theta/2\theta$ scan technique with a locally modified Picker four-circle goniostat equipped with a Furnas monochromator (HOG crystal) and Mo source (λ = 0.710 69 Å). The scan speed was 3°/min. The scan width was 2° plus dispersion. The data set was collected out to 2θ = 50°, giving 3953 unique reflections of which 3647 with $F > 2.33\sigma(F)$ were used for the structure determination. An absorption correction was applied based on a linear absorption coefficient of 103.7 cm^{-1}.

Table IX. Calculated Fractional Hydrogen Atom Coordinates[a]

atom	x	y	z
H(A)	0.332 781	0.418 959	0.972 084
H(B)	0.195 135	0.320 196	0.716 474
H(C)	0.264 764	0.293 672	0.936 662
H(1)	0.257 03	0.118 09	0.894 63
H(2)	0.164 21	0.153 25	1.001 64
H(3)	−0.010 46	0.206 65	0.757 14
H(4)	−0.011 01	0.203 40	0.518 58
H(5)	0.156 90	0.159 63	0.606 66
H(6)	0.238 93	0.494 74	0.951 71
H(7)	0.150 90	0.491 82	0.660 33
H(8)	−0.014 51	0.400 88	0.527 01
H(9)	−0.025 21	0.371 23	0.748 00
H(10)	0.132 83	0.408 13	1.008 14
H(11)	0.280 18	0.276 86	0.694 11
H(12)	0.389 47	0.134 82	0.887 10
H(13)	0.547 65	0.220 29	1.101 55
H(14)	0.542 53	0.401 30	1.042 84
H(15)	0.373 12	0.445 86	0.811 31
H(16)	0.275 90	0.307 80	1.155 90
H(17)	0.389 87	0.157 07	1.207 61
H(18)	0.546 43	0.230 56	1.292 96
H(19)	0.539 32	0.418 79	1.292 64
H(20)	0.382 10	0.460 44	1.230 92

[a] The hydrogens on the Cp ligands were placed at a bond distance of 1.080 Å. See ref 22.

Table X. Calculated Hydride Bond Distances

A	B	distance, Å
W(1)	H(B)	1.615
W(1)	H(C)	1.861
W(2)	H(C)	1.852
W(2)	H(A)	1.593

The structure was solved by a combination of Patterson and direct methods.[39] Initial attempts to refine the structure using the data as obtained yielded nonpositive definite thermal parameters for eight of the anisotropic thermal parameters (Table XIV, supplementary material). After correcting for absorption, the refinement still yielded a nonpositive thermal parameter for C(3). This is undoubtedly due to either an incorrect absorption correction or a slight decomposition of the sample.

There was no indication of disorder in either the acetone of crystallization or the perchlorate counterion. The hydrogen positions were not located directly. The final discrepancy factors were $R = 0.0706$ and $R_w = 0.1113$. The maximum δ/σ for the last cycle was 0.15.

Hydrogen positions were placed in "calculated" positions in the molecule shown in Figure 9, by assuming that the geometry of each half of the molecule closely resembled that of Cp_2MoH_2.[22] A "best molecular fit" was obtained by least-squares treatment[40] in which the coordinates of the nonhydrogen atoms in the latter molecule were transformed to our unit cell and translated and rotated so that the sums of the distances between the corresponding carbons of the two cyclopentadienyl rings and the metals were minimized. The coordinates of the two hydride ligands of Cp_2MoH_2 were then assumed to correspond to hydrogen positions in our cell. The coordinates of the bridging hydrogen were taken as the simple average of the two hydrogens which were located near the center of the W–W axis. The results are presented in Tables IX and X.

Acknowledgment. We wish to thank Dr. G. D. Stucky for permission to reproduce the structure of Cp_2MoH_2, the M. H. Wrubel Computing Center for computational facilities, and the National Science Foundation for generous financial support.

Supplementary Material Available: Complete listing of bond distances (Table XI) and bond angles (Table XII), listing of observed and calculated structure factors (Table XIII), and listing of anisotropic thermal parameters (Table XIV) (41 pages). Ordering information is given on any current masthead page.

References and Notes

(1) (a) Cotton, F. A.; Wilkinson, G. "Advanced Inorganic Chemistry", 3rd ed.; Interscience: New York, 1972; Chapter 24. (b) Tolman, C. A. In "Transition Metal Hydrides", E. L. Muetterties, Ed.; Marcel Dekker: New York, 1971; p 271. (c) Labinger, J. A. *Adv. Chem. Ser.* **1977**, *167*, 149. (d) Ford, P. C.; Rinker, R. G.; Ungermann, C.; Laine, R. M.; Landis, V.; Moya, S. A. *J. Am. Chem. Soc.* **1978**, *100*, 4595.
(2) Klingler, R. J.; Mochida, K.; Kochi, J. K. *J. Am. Chem. Soc.*, **101**, 6626 (1979).
(3) Compare (a) Green, J. C.; Jackson, S. E.; Higginson, B. *J. Chem. Soc., Dalton Trans.* **1975**, 403. (b) Cradock, S.; Ebsworth, E. A. V.; Robertson, A. *Ibid.* **1973**, 23. (c) Higginson, B. R.; Lloyd, D. R.; Evans, S.; Orchard, A. F. *J. Chem. Soc., Faraday Trans. 2*, **1975**, *71*, 1913.
(4) dmpe = bis(dimethylphosphino)ethane ($Me_2PCH_2CH_2PMe_2$); diphos = bis(diphenylphosphino)ethane ($Ph_2PCH_2CH_2PPh_2$); Cp = cyclopentadienyl.
(5) Kenkel, J. V.; Bard, A. *J. Electroanal. Chem. Interfacial Electrochem.* **1974**, *54*, 47.
(6) The proton splittings *in* Cp_2NbH_2 and $Cp_2NbH(t\text{-}Bu)$ *are* 11.7 and 11.6 G, respectively. For that in some other metal hydrides see Elson, I. H.; Kochi, J. K.; Klabunde, U.; Manzer, L. E.; Parshall, G. W.; Tebbe, F. N. *J. Am. Chem. Soc.* **1974**, *96*, 7374.
(7) Mochida, K.; Kochi, J. K.; Chen, K. S.; Wan, J. K. *J. Am. Chem. Soc.* **1978**, *100*, 2927.
(8) Nadjo, L.; Saveant, J. M. *J. Electroanal. Chem.* **1973**, *48*, 113.
(9) King, R. B. "Organometallic Synthesis"; Academic Press: New York, 1965; p 109.
(10) (a) Kaesz, H. D.; Saillant, R. B. *Chem. Rev.* **1972**, *72*, 231. (b) Cooper, C. B., III; Shriver, D. F.; Onaka, S. *Adv. Chem. Ser.* **1978**, *167*, 232.
(11) Adams, R. D.; Collins, D. M.; Cotton, F. A. *Inorg. Chem.* **1974**, *13*, 1086.
(12) Schunn, R. A. In ref 1b, p 238.
(13) (a) Fischer, E. O.; Hristidu, Y. *Z. Naturforsch. B* **1960**, *15*, 135. (b) Greer M. L. H.; McCleverty, J. A.; Pratt, L.; Wilkinson, G. *J. Chem. Soc.* **1961**, 4854. (c) Compare also Kotz, J. C.; Pedrotty, D. G. *J. Organomet. Chem.* **1970**, *22*, 425.
(14) (a) Hughey, J. L., IV; Bock, C. R.; Meyer, T. J. *J. Am. Chem. Soc.* **1975**, *97*, 4440. (b) Wrighton, M. S.; Ginley, D. S. *ibid.* **1975**, *97*, 3534.
(15) Compare Davison, A.; Wreford, S. S. *J. Am. Chem. Soc.* **1974**, *96*, 3017.
(16) (a) Baker, E. C.; Raymond, K. N.; Marks, T. J.; Wachter, W. A. *J. Am. Chem. Soc.* **1974**, *96*, 7586. (b) Marks, T. J.; Seyam, A. M.; Kolb, J. R. *Ibid.* **1973**, *95*, 5529. (c) Marks, T. J.; Wachter, W. A. *Ibid.* **1976**, *98*, 703.
(17) (a) For other modes of reductive elimination see Geoffroy, G. L.; Bradley, M. C.; Pierantozzi, R. *Adv. Chem. Ser.* **1978**, *167*, 181. Tsou, T. T.; Kochi, J. K. *J. Am. Chem. Soc.* **1978**, *100*, 1634. (b) It is noteworthy that paramagnetic radical ions of the group 4 A metal hydrides such as Bu_3SnH^+ fragment by loss of hydrogen atom (i.e., $\rightarrow H\cdot + Bu_3Sn^+$); see ref 2.
(18) For a ^1H NMR and IR of bridging hydrides see the Results section.
(19) Olsen, J. P.; Koetzle, T. F.; Kirtley, S. W.; Andrews, M. A.; Tipton, D. L.; Bau, R. *J. Am. Chem. Soc.* **1974**, *96*, 6621.
(20) Hart, D. W.; Bau, R.; Koetzle, T. F., to be published. Cited in Bau, R.; Teller, R. G.; Kirtley, S. W.; Koetzle, T. F. *Acc. Chem. Res.* **1979**, *12*, 176.
(21) Love, R. A.; Chin, H. B.; Koetzle, T. F.; Kirtley, S. W.; Whittlesey, B. R.; Bau, R. *J. Am. Chem. Soc.* **1976**, *98*, 4491.
(22) Schultz, A. J.; Stearley, K. L.; Williams, J. M.; Mink, R.; Stucky, G. D. *Inorg. Chem.* **1977**, *16*, 3303.
(23) For an appropriate comparison, see ref 11. The structure of the related $Cp_2WH_2^+$ has been reported, but the hydridic ligands were not located.[24]
(24) Bau, R.; Carroll, W. E.; Teller, R. G.; Koetzle, T. F. *J. Am. Chem. Soc.* **1977**, *99*, 3872.
(25) Wilson, R. D.; Koetzle, T. F.; Hart, D. W.; Kvick, A.; Tipton, D. L.; Bau, R. *J. Am. Chem. Soc.* **1977**, *99*, 1775.
(26) Interpreted as due to the high ligand field strength of the hydride [Geoffroy, G. L.; Bradley, M. C.; Pierantozzi, R. *Adv. Chem. Ser.* **1978**, *167*, 181].
(27) A general electronic spectral feature of all singly bonded M–M units is an intense $\sigma \rightarrow \sigma^*$ absorption,[28] but the assignment of the bridged M–H–M system is more complicated.[29]
(28) Trogler, W. C.; Gray, H. B. *Acc. Chem. Res.* **1978**, *11*, 232, and references cited therein.
(29) Harris, D. C.; Gray, H. B. *Inorg. Chem.* **1975**, *14*, 1215.
(30) Francis, B. R.; Green, M. L. H.; Roberts, G. G. *Chem. Commun.* **1971**, 1290.
(31) (a) Fairugia, L.; Green, M. L. H. *J. Chem. Soc., Chem. Commun.* **1975**, 416. (b) Elmit, K.; Green, M. L. H.; Forder, R. A.; Jefferson, I.; Prout, K. *Ibid.* **1974**, 747. (c) Giannotti, C.; Green, M. L. H. *Ibid.* **1972**, 1114.
(32) Aresta, M.; Giannocaro, P.; Rossi, M.; Sacco, A. *Inorg. Chim. Acta* **1971**, *5*, 115.
(33) Van Duyne, R. P.; Reilley, C. N. *Anal. Chem.* **1972**, *44*, 142.
(34) Manriquez, J. M.; Fagan, P. J.; Marks, T. J. *J. Am. Chem. Soc.* **1978**, *100*, 3939.
(35) Although the relevance of pH readings in nonaqueous solutions is difficult to define [Harlow, G. A.; Noble, C. M.; Wyld, G. E. A. *Anal. Chem.* **1956**, *28*, 787], calibration allows meaningful interpretations to be made.
(36) See ref 33 for similar observations and an extensive discussion of low-temperature electrochemistry.
(37) Bauer, H. H.; Elving, P. J. *J. Am. Chem. Soc.* **1960**, *82*, 2091.
(38) Smith, D. E. *Electroanal. Chem.* **1966**, *1*, 1.
(39) All computations were performed on a CYBER 172/CDC 6600 multiframe system using the Indiana University Molecular Structure Center XTEL interactive library. The latter is based on codes from J. A. Ibers (Northwestern University) and A. C. Larson (LASL), as well as local codes.
(40) Nyburg, S. C. *Acta Crystallogr., Sect. B.* **1974**, *30*, 251.